Edge-of-contact stresses in blade attachments in gas turbines

G. B. Sinclair
Department of Mechanical Engineering, Louisiana State University, USA

Abstract

By drawing on analytical solutions to contact problems in the literature, an approach is developed for obtaining two-dimensional, elastic, edge-of-contact stresses in blade attachments in gas turbines. The approach is validated on a benchmark problem. It uses stress resultants from finite element analysis (FEA): stress resultants converge more rapidly than stresses themselves, so that such FEA is less demanding. In addition to reducing FEA, the analytical approach reveals with explicit expressions the nature of edge-of-contact stresses in blade attachments. In particular in this regard, it identifies a hoop stress component right at the edge of contact that is potentially damaging to blades.
Keywords: two-dimensional conforming contact, contact with friction, elastic contact stresses.

1 Introduction

At this time, gas turbine engines are the norm for powering larger planes in commercial and military use. In addition, land-based gas turbines have largely replaced reciprocating engines as power generators. Essential to the success of gas turbines in both roles has been the engineering of sufficient structural reliability. A key aspect of this engineering effort has been the design of fan blade attachments to fan hubs or rotors. While the structural integrity of these attachments has improved with time, failures do still occur. The intent of the work reported here, then, is to offer a means of gaining increased understanding of the critical edge-of-contact stresses occurring in blade attachments in gas turbines: such understanding can aid in achieving yet better structural integrity of attachments.

WIT Transactions on Engineering Sciences, Vol 78, © 2013 WIT Press
www.witpress.com, ISSN 1743-3533 (on-line)
doi:10.2495/SECM130081

A cross section of a typical dovetail blade attachment used in aircraft engines is shown in fig. 1. Therein the base of one blade in a fan is restrained from moving radially outward (upwards in fig. 1) when rotating by contact on two flats (*C*-*C*' in fig. 1) within its portion of the rotor. Attachments of this ilk are common in the aircraft industry. Fir tree attachments with multiple pairs of contacting flats are also used in the industry, as well as in power generation.

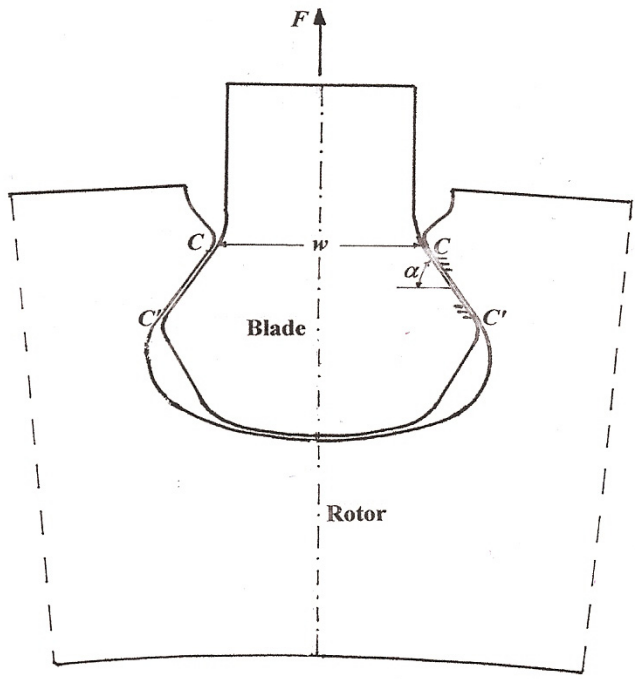

Figure 1: Cross section of a dovetail attachment of a blade base to a rotor.

With slipping on the contact flats during loading up to peak rpm, tensile edge-of-contact stresses are produced in the blade and the rotor (at *C* and *C*', respectively, in fig. 1). With even minor variations in operating rpm, these tensile stresses can fluctuate significantly and thus initiate fatigue cracks that ultimately lead to failure. Understanding these tensile edge-of-contact stresses that are the root causes of these failures is of fundamental importance in trying to design against failures.

Finite element analysis (FEA) offers a means of making a determination of the edge-of-contact stresses in blade attachments under varying operating conditions. One of the attributes of FEA is its ability to simulate entire geometries like that shown in fig. 1. Nonetheless, FEA faces some challenges in accurately resolving the local edge-of-contact stresses present. In the first instance this is because these stresses have high gradients, indeed even infinite

gradients right at the edge of contact. In the second this is because the expanded contact region within which the peak contact stresses occur is itself quite small (typically about 1% of the contact flat at maximum rpm). Thus FEA must not only resolve stresses with severe gradients but also make a sufficiently accurate determination of the region within which these stresses act.

Over the years a number of papers have reported attempts to use FEA to capture edge-of-contact stresses in blade attachments in gas turbines (see Sinclair *et al*. [1] for references). These finite element treatments are all within the context of two-dimensional elasticity. The most refined mesh employed has contact elements with extents that are of the order of 1/100 of the edge radius, itself a small dimension. While results from this FEA are consistent with a numerical analysis that has converged to within 4% for some of the edge-of-contact stresses, for the crucial tensile stress convergence remains problematic.

Here, therefore, we adopt a different approach. We use FEA to its best advantage, namely simulating an entire geometry like that of fig. 1, but then only require the FEA to determine stress resultants on contact flats. Being integrals of stresses, resultants are far less sensitive to severe stress gradients, and are also fairly insensitive to precise extents of contact. Thereafter we use an analytical approach to obtain edge-of-contact stresses. This analytical approach is based on an adaptation of the two-dimensional, closed-form, elastic solution for a flat punch with rounded edges indenting an elastic half plane given in Shtaerman [2]. The intent of employing this analytical approach is not only to improve the resolution of edge-of-contact tensile stresses but also to increase understanding of edge-of-contact stresses by furnishing some closed-form expressions for key contributions.

In what follows, we begin in Section 2 by describing in greater detail the specific blade attachment used to demonstrate the application of the analytical approach. Thereafter, in Sections 3, 4 and 5, we develop the analytical approach used for the contact stress then other edge-of-contact stresses. To validate the approach, in Section 6 we compare with what we believe to be the most accurately determined edge-of-contact stresses found with FEA. We close in Section 7 with remarks on some consequences of the approach in general.

2 Contact configuration

The cross section of a dovetail blade attachment shown in fig. 1 is, in fact, the one chosen for demonstrating the analytical approach developed subsequently. This choice is primarily because this is the attachment that has been subjected to the most refined FEA we are aware of in [1]: in addition, we can obtain the necessary specifications from [1] for this attachment.

The cross section in fig. 1 is assumed to be in a state of plane strain out of the plane of the figure. Furthermore, the force F induced by the rotation of the blade is assumed to be shared equally by the two contacting flats restraining the blade. Then the cross section in fig. 1 is symmetric about its center line, and it suffices to consider but one of the contacting flats.

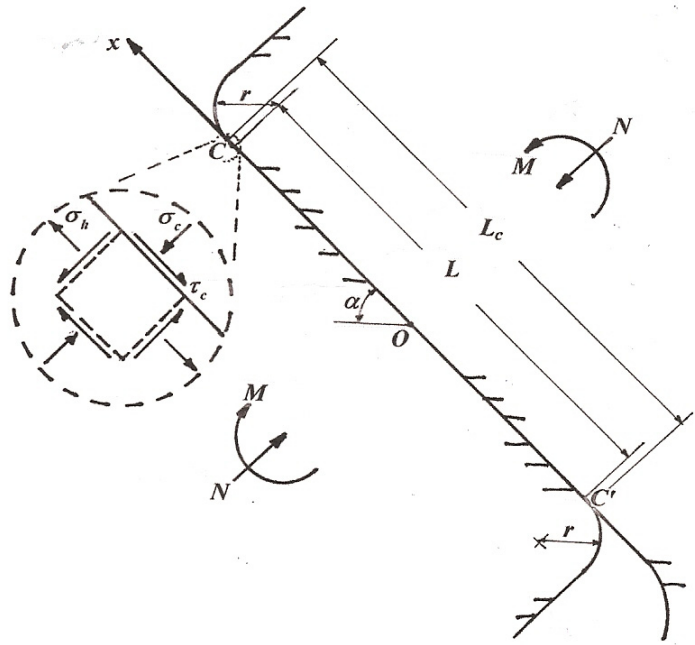

Figure 2: Contact geometry and coordinate; local stresses.

The local contact configuration for the right most restraining flat is shown in greater detail in fig. 2. Therein L is the length of the contact flat that is common to both the blade and the rotor, and this flat is inclined at an angle α to the horizontal direction. At the ends of this flat there is a common edge radius r, on the rotor at the upper end and on the blade at the lower. Under loading, actual contact expands a small amount onto these radii, shown schematically as extending to C and C' in fig. 2: the horizontal distance between C and C' is denoted as the contact length L_c. To describe variations of stresses within L_c, a coordinate x aligned with the contact flat and having origin O at the center of the flat is introduced.

Contact between the blade and the rotor extending over the flat in fig. 2 is produced by a normal pressure acting in concert with a bending stress. For the first of these, the associated nominal pressure on the contact flat is given by

$$p = N/L, N = F/2\left(\cos\alpha + \mu\sin\alpha\right), \tag{1}$$

where N is the resultant normal force on a contact flat and μ is the coefficient of friction between the blade and the rotor. In eqn (1), slipping between the blade and the rotor has been assumed (we review some justification for this assumption subsequently in Section 5). For the second of these, the associated nominal stress is

$$\sigma_m = 2\sigma x/L, \sigma = 6M/L^2, \tag{2}$$

where M is the resultant moment acting and is taken to be positive when adding to N at $x = L/2$.

For the dovetail attachment of fig. 1, F follows from the geometry and density of the blade, as well as the rotational speed at which the fan operates. For M, on the other hand, analysis is required because this moment is statically indeterminate. Since M is a stress resultant rather than a stress, this analysis can be fairly readily performed with 2D or even 3D finite elements. (For some other blade attachments, such as fir tree attachments, F may also have to be determined using FEA.)

Our general objective here, then, is to determine the stresses produced in the blade and the rotor under the action of N and M that satisfy: the field equations of plane-strain elasticity, matched tractions and normal displacements within the contact region, Amonton's law within the contact region, stress-free conditions outside of the contact region, and the usual contact constraints. These last require that the contact stress between the blade and the rotor be nowhere tensile, and that displacements of the blade and the rotor do not let the two touch outside of the contact region.

In particular, we are interested in the local stresses at or near the edge of contact. There are three stress components of principal interest in this vicinity: the normal contact stress σ_c, the companion shear contact stress τ_c, and the normal hoop stress σ_h. These are shown acting in their adopted positive senses in the close-up in fig. 2. Thus σ_c is positive when compressive, which it always is, while σ_h has the more normal sign convention of being positive when tensile because it can be both tensile and compressive.

The actual dovetail attachment in [1] is one used by General Electric Aircraft Engines and is made with a titanium alloy. For this attachment,

$$r/L = 7/52, \alpha = \tan^{-1} 17/12. \tag{3}$$

As in [1], we consider two limiting cases for friction effects: $\mu = 0.0$ and $\mu = 0.4$. The first of these is for the minimum coefficient for frictionless operation, while the second is for the maximum coefficient estimated to occur in dovetail attachments when they are made with the titanium alloy (see Hamdy and Waterhouse [3]). Then, as in [1], corresponding loading has

$$p/E_c = 5.66 \times 10^{-3}, 3.61 \times 10^{-3}, \tag{4}$$

for $\mu = 0.0, 0.4$, respectively. In eqn (4), E_c is the contact modulus and is defined by

$$E_c = \left(\frac{1-\nu_b^2}{E_b} + \frac{1-\nu_r^2}{E_r} \right)^{-1}, \tag{5}$$

where E_b and ν_b are the Young's modulus and Poisson's ratio for the blade, E_r and ν_r like moduli for the rotor.

3 An analytical approach for the contact stress absent bending effects

Here we adapt the analytical solution of Shtaerman [2] so as to furnish estimates of the contact stress σ_c in fig. 2 produced by the nominal pressure p alone. Initially we do this for the frictionless case: later, in Section 5, we discuss the effects of friction.

A cross section of the plane-strain contact configuration analyzed in Shtaerman [2] is shown in fig. 3(a). Therein a rigid smooth punch is pressed by a normal force into an elastic half plane. The punch has a flat base with rounded edges: we take the extent of the flat to equal L and the edge radii to equal r in common with the contact configuration of fig. 2. Then we take the magnitude of the remote forces pushing the two together to be N in order to have a nominal pressure of p on the contact flat. The half plane has a Young's modulus E and a Poisson's ratio ν. In fig. 3(a), we continue to employ an x coordinate arranged as earlier in fig. 2.

By superimposing displacements from the Flamant line load on an elastic half plane, the contact stress acting in fig. 3(a) can be shown to satisfy the integral equation

$$\frac{1-\nu^2}{E}\, I(x) = u_P(x), \tag{6}$$

for $|x| < L_c/2$, where L_c is now the contact extent in Shtaerman's problem ($L_c > L$). In eqn (6), I is the integral resulting from the superposition of line loads, and u_P is the displacement produced in the half plane by the punch profile. Thus from, for example, Johnson [4], p. 17,

$$I(x) = \frac{-2}{\pi} \int_{-L_c/2}^{L_c/2} \sigma_c(\xi) \ln\left|\frac{x-\xi}{L_c}\right| d\xi, \tag{7}$$

and u_P, using the approximation of Hertz [5], is given by

$$u_P(x) = \begin{cases} \delta & \text{for } |x| \le L/2, \\ \delta - (2x-L)^2/8r & \text{for } L/2 < |x| \le L_c/2, \end{cases} \tag{8}$$

wherein δ is the depth of penetration of the punch flat.

In eqn (6), it is understood that σ_c must be positive to be in compliance with the contact constraint requiring contact stresses be compressive. Further in eqn (6), L_c is to be adjusted so that the half-plane displacements outside of the contact region do not touch the punch and so are in compliance with the second contact constraint.

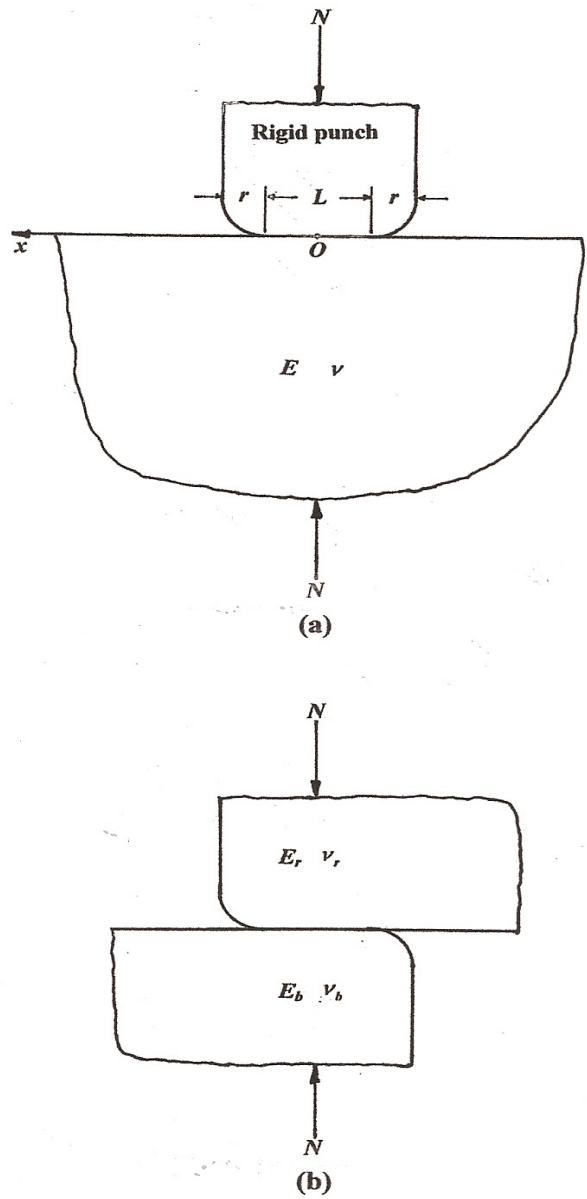

Figure 3: Shtaerman contact configurations – (a) original configuration, (b) modified equivalent configuration.

To adapt this integral equation so that it applies to the contact configuration of fig. 2, we first let the half plane replicate the blade and hence replace E and ν by corresponding values for the blade, E_b and ν_b. Next we let the punch be

deformable with moduli E_r and ν_r. Then the displacements produced in punch are to be subtracted off u_P on the right-hand side of eqn (6). Following Steuermann [6], we let these displacements also be represented by those attributable to the superposition of half-plane line loads. Accordingly, with both of these modifications, eqn (6) becomes

$$\frac{1-\nu_b^2}{E_b} I(x) = u_P(x) - \frac{1-\nu_r^2}{E_r} I(x), \tag{9}$$

for $|x| < L_c/2$. That $I(x)$ on the right-hand side of eqn (9) remains the same as in eqn (7) is a consequence of assuming the same Green's function for the half plane and the punch, together with the fact that both are acted on by the same contact stress. The assumption of a common Green's function, as well as the Hertz approximation used in eqn (8), are only reasonable provided the expansion of the contact area does not progress too far around the edge radii. In Persson [7], an assessment is made of the extent that contact can extend and have to two simplifications remains reasonable. Somewhat surprisingly, [7] finds this to be the case provided contact regions do not extend horizontally more than 40% of contact radii. Because we expect lateral contact extensions to be less than this for the present class of contact problems, the two simplifications can be expected to be reasonable here. We do, though, check that this is indeed the case subsequently.

Returning to eqn (9) and rearranging it by placing both I terms on the left-hand side, we see that the only change to the original integral equation for Shtaerman's problem, eqn (6), is that the coefficient of I, $\left(1-\nu^2\right)/E$, is replaced by E_c^{-1} where E_c is the contact modulus of eqn (5). It follows that the only change needed to be made to Shtaerman's solution for eqn (6) so that it applies to a deformable punch and half plane respectively having the moduli of the rotor and the blade is the aforementioned exchange.

Finally in adapting the configuration of fig. 3(a) to that of fig. 2, we note that the punch profile u_p can equally well be interpreted as the amount the indentor would overlap or interpenetrate the half plane were it not for the compensating displacements in eqn (9). With this interpretation, it is of no consequence whether u_p comes from interpenetration of the punch into the half plane or vice versa. For that matter, the punch could interpenetrate the half plane for a portion of the contact region and the half plane interpenetrate the punch for the remainder and eqn (9) would remain unchanged. Hence eqn (9) holds in effect for the configuration of fig. 3(b), and therefore the Shtaerman's solution for eqn (6) applies for the contact stress in fig. 2 provided the noted moduli exchange is made. Accordingly for this contact stress, from Shtaerman [2],

$$\sigma_c = \frac{E_c L_c}{\pi r}\left[\Phi\sin\phi + \ln\sqrt{\left(\left|\frac{\sin(\Phi+\phi)}{\sin(\Phi-\phi)}\right|^{\cos\phi}\left|\frac{\sin\Phi-\sin\phi}{\sin\Phi+\sin\phi}\right|^{\cos\Phi}\right)}\right], \tag{10}$$

for $|x| \le L_c/2$, where

$$\phi = \cos^{-1}\left(2x/L_c\right),\ \Phi = \cos^{-1}\lambda, \lambda = L/L_c\,. \tag{11}$$

To quantify σ_c using eqn (10), the contact length L_c needs to be determined. Also from Shtaerman [2], this can be effected by solving

$$8pr\lambda^2 = E_c L\left(\Phi - \lambda\sin\Phi\right) \tag{12}$$

for λ, hence Φ and L_c. This transcendental equation can be readily solved numerically.

By way of example, for the edge radius of eqn (3) and the frictionless loading of eqn (4), solving eqn (12) with the secant method yields

$$\lambda = 0.9787. \tag{13}$$

This corresponds to $\Delta L_c/r$ equal to 8%, where $\Delta L_c = \left(L_c - L\right)/2$ is the lateral contact extension for a single end of the contact region. This is markedly less than the percentage assessed as acceptable in Persson [7]. With λ of eqn (13) and hence Φ of eqn (11), σ_c of eqn (10) can be evaluated when normalized by p. This leads to the contact stress distribution shown in fig. 4(a) for $0 \le x \le L_c/2$ (the distribution for $x < 0$ is simply a reflection because σ_c of eqn (10) is symmetric about $x = 0$). This stress distribution features a sharp peak within the contact region extension onto the rounded edge.

By differentiating eqn (10) with respect to x and setting $d\sigma_c/dx = 0$, the location of the maximum contact stress, σ_c^+, can be found. Thus $\sigma_c^+ = \sigma_c\left(\phi = \phi^+\right)$, where ϕ^+ results from solving

$$2\Phi\cot\phi^+ = \ln\left(\frac{\sin\left(\Phi + \phi^+\right)}{\sin\left(\Phi - \phi^+\right)}\right), \tag{14}$$

for $\phi^+ < \Phi$. This transcendental equation can also be readily solved numerically. For the same frictionless case as for λ of eqn (13), this leads to $\phi^+ = 9.873°$. Using eqn (13), this corresponds to

$$2x^+/L = 1.0066, \tag{15}$$

where x^+ is the location of σ_c^+. That is, the maximum contact stress occurs but 1/3 of a percent of the length of the contact flat outside of this flat. At this location, eqn (10) has

$$\sigma_c^+/p = 5.46. \tag{16}$$

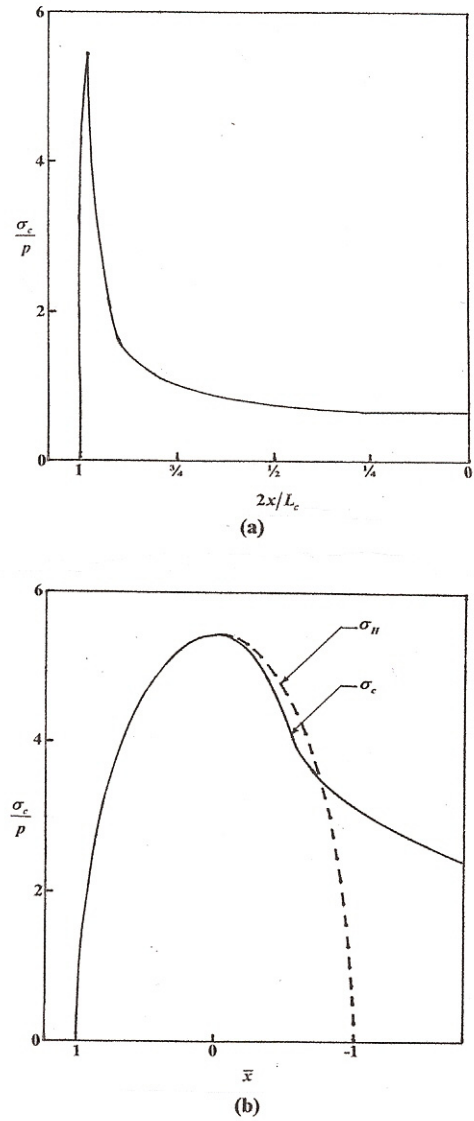

Figure 4: Representative contact stress $(\mu = 0)$: (a) stress distribution over half of the contact region; (b) edge-of contact stress.

The stress distribution near this maximum is shown more clearly in the close up of this vicinity in fig. 4(b).

Included in fig. 4(b), starting at the edge of contact $x = L_c/2$, is a local Hertzian contact stress distribution sharing the same peak stress as σ_c. After Hertz [5] for a cylindrical roller, this stress is given by

$$\sigma_H = \sigma_c^+ \sqrt{\left(1 - \overline{x}^2\right)}, \tag{17}$$

for $|\overline{x}| \le 1$, where $\overline{x} = \left(x - x^+\right)\big/\Delta x^+$ and $\Delta x^+ = \left(L_c/2\right) - x^+$. The Hertzian stress of eqn (17) agrees with σ_c for $0 \le \overline{x} \le 1$ corresponding to $x^+ \le x \le L_c/2$ to within 1%. This is not surprising since σ_c and σ_H share both the same stress values and the same stress gradients at $x = x^+$ and $L_c/2$. We take advantage of this agreement between the two later when we assemble contributions to the hoop stress, σ_h.

4 An adjustment to the contact stress to reflect bending effects

At the outset in attempting to incorporate the effects of bending, we assume that these are not of a sufficient magnitude to negate the compressive nature of the contact stresses produced by uniform pressures and thereby lead to lift off and separation in the contact region. For flat punches with sharp edges Gladwell [8], p. 74, has that such will be the case if σ of eqn (2) is limited by

$$\sigma/p < 3/2. \tag{18}$$

In lieu of any more appropriate limit, we adopt that of eqn (18) in what follows.

Fortunately for the dovetail attachment in [1], while nominal bending stresses are appreciable, they are not close to the limit imposed by eqn (18). For this attachment, Sinclair and Cormier [9] reports that

$$\sigma/p = 0.36, 0.58, \tag{19}$$

for $\mu = 0.0, 0.4$, respectively. Furthermore, for fir tree attachments, nominal bending stresses are relatively modest, and so also in compliance with eqn (18).

Unfortunately for punches with rounded edges as in fig. 3(a), the bending counterpart to eqn (10) would not appear to be available in the literature. There are, however, analytical solutions for σ_c for both p and σ_m when the punch is completely flat with sharp edges. For p, σ_c is given in Sadowsky [10], while for σ_m, σ_c is given in Gladwell [8]. Accordingly we next try to take advantage of these flat punch solutions to arrive at an estimate of the effects of additional bending contributions on contact stresses for punches with small radii rounding their edges $\left(r/L \le 1/5\right)$.

From Sadowsky [10], when a smooth flat punch of width L is pressed by a uniform pressure p into an elastic half plane, the contact stress σ_f produced is given by

$$\sigma_f = \frac{2p}{\pi\sqrt{1-(2x/L)^2}}, \tag{20}$$

for $|x| < L/2$, where x continues to be as in fig. 3(a). Now $L_c = L$ because of the sharp corners, and stress singularities occur at the edges of contact. From Gladwell [8], the corresponding result for the same configuration but now with σ_m acting on the punch is σ_{fm} where

$$\sigma_{fm} = \frac{4\sigma}{3\pi\sqrt{1-(2x/L)^2}}\,\frac{2x}{L}, \tag{21}$$

for $|x| < L/2$. Now it is assumed that σ_m acts in concert with sufficient p that contact is preserved over $|x| < L/2$, and again $L_c = L$. For this to be the case, $|\sigma_{fm}|$ should be less that σ_f : this is so when eqn (18) holds. The contact stress of eqn (21) shares the same stress singularity as its predecessor in eqn (20). Hence the quotient σ_{fm}/σ_f has a finite limit as $x \to L/2$. If we let σ_f^+ denote the peak stresses in the vicinity of $x = L/2$ for p alone and σ_{fm}^+ the corresponding stress for p in concert with σ_m, eqns (20) and (21) give

$$\frac{\sigma_{fm}^+}{\sigma_f^+} = 1 + \frac{2\sigma}{3p}. \tag{22}$$

Thus the right-hand side of eqn (22) is the factor that peak contact stresses for flat punches are increased by as the result of bending contributions.

The contact stress of eqn (20) for the punch with sharp corners agrees with its counterpart of eqn (10) for the punch with corners rounded in accord with eqn (3) to within 3% over the central 90% of the contact region. Outside of this central region, significant differences in contact stresses occur for the two punches. However, because the stresses agree for the central 90%, the two punches must share common forces acting thereon. Hence, since they share common total forces, they must also share common forces acting on their outer regions. It follows, therefore, that the factor in eqn (22) reflects the increase in applied forces acting on the outer contact regions as a result of bending effects.

For the Hertzian contact of a cylinder, increasing the applied force or p has the peak contact stresses, σ_H^+, increase proportional to $p^{1/2}$ (see, e.g., [4], p. 427). This is because increases in p are mitigated to a degree by expansions in the

contact region. Thus if we accept the factor in eqn (22) as being that for increasing load with bending, we would have

$$\frac{\sigma_{Hm}^{+}}{\sigma_{H}^{+}} = \left(1+\frac{2\sigma}{3p}\right)^{1/2}, \tag{23}$$

where σ_{Hm}^{+} is a notional peak Hertzian contact stress with bending present.

While the outer edges of a punch with rounded corners do have a similar stress distribution to that for Hertzian contact of a cylinder, inside the common peak value of this stress the stresses for the two differ appreciably. In part this is because the punch with rounded corners only enjoys stress relief from expanding contact from expansions on one side of the peak contact stress. Accordingly we can expect the factor for increasing stresses due to bending for a punch with rounded corners to lie somewhere between that of eqn (22) for punches with sharp corners and that of eqn (23) for cylinders.

In an attempt to obtain this intervening factor, we track σ_{c}^{+} from eqns (10), (11), (12) and (14) as p varies throughout the range given in eqn (4). We find that σ_{c}^{+} is consistently proportional to $p^{2/3}$ over this range. Consequently for punches with rounded corners we take

$$\frac{\sigma_{cm}^{+}}{\sigma_{c}^{+}} = \left(1+\frac{2\sigma}{3p}\right)^{2/3}, \tag{24}$$

where σ_{cm}^{+} is σ_{c}^{+} when σ_{m} acts as well as p. Then, for the nominal stress ratios of eqn (19), we have

$$\sigma_{cm}^{+}/\sigma_{c}^{+} = 1.154, 1.244, \tag{25}$$

for μ = 0.0, 0.4, respectively. Thus with bending the maximum contact stress of eqn (16) is increased to

$$\sigma_{cm}^{+}/p = 6.30, \tag{26}$$

when there is no friction. We give the corresponding increases for when friction acts after we discuss contact shear stress influences in the next section. Once σ_{cm}^{+} is determined, paralleling eqn (21), for the entire contact stress distribution with bending present, we take

$$\sigma_{cm} = \sigma_{c}\left[1+\frac{2x}{L}\left(\frac{\sigma_{cm}^{+}}{\sigma_{c}^{+}}-1\right)\right], \tag{27}$$

for $|x| \le L_{c}/2$, with σ_{c} remaining as given by eqn (10).

5 An analytical approach for the other edge-of-contact stresses

Here we first make a determination of the shear contact stress, τ_c, for the configuration of fig. 2. Thereafter we combine the effects of τ_c with those of σ_c and *F* in making a determination of the hoop stress, σ_h.

In Sinclair and Cormier [9], a simple cork model indicates that attachments like that of fig. 1 can be expected to slip as loading up commences if

$$\tan\alpha > \mu. \tag{28}$$

Equation (28) is certainly complied with here (see eqn (3)), and this is typically the case for other blade attachments.

In [1], the FEA finds the blade in the attachment of fig. 1 not only to start to slip during loading up, but also to continue slipping throughout loading. Here, then, we assume this to be the case. However, this is an assumption that really needs to be confirmed for other attachments, something that is fairly readily done with FEA. (Griffin and Cushman [11] reports the same finding of slipping throughout loading for a firtree attachment.)

Under the assumption of slipping, Amonton's law applied at the stress level has

$$\tau_c = \mu\sigma_c, \tag{29}$$

for $|x| \le L_c/2$ when there is no bending present. With bending, eqn (29) simply becomes

$$\tau_{cm} = \mu\sigma_{cm}, \tag{30}$$

for $|x| \le L_c/2$, where τ_{cm} is the shear stress with σ_m acting as well as *p*. Some justification for the application of Amonton's law at the stress level rather than for forces is given in Johnson [4], on p. 204.

Unfortunately there would not appear to be a solution in the literature for σ_c for punches with rounded corners when eqn (29) holds. There is, though, a solution for a punch with sharp corners when eqn (29) holds given in Muskhelishvili [12] on p. 497. Because of the sharp corners, this solution has stress singularities at the edges of contact. Moreover, because of the different boundary conditions involved, these singularities do not share the same singularity exponent as punches with sharp corners absent friction (see eqn (20)). Hence it is only appropriate to compare contact stresses for punches with sharp corners and with and without friction well away from the edges of contact. With this restriction, it is found that the contact stresses with and without friction are quite similar. More precisely for μ = 0.0 and 0.4 when $|x| < L_c/4$, differences in σ_c are less than 4%. Accordingly here we choose to ignore any frictional

effects on contact stress distributions and take σ_c of eqn (10) to apply in eqn (29), σ_{cm} of eqn (27) in eqn (30).

On the other hand, with friction there are differences in applied nominal pressures because some of the force *F* is now balanced by shear stress resultants. These enter through eqn (1) and result in the reduced *p* with friction given in eqn (4). For this *p*, eqn (12) leads to $\lambda = 0.9840$ and an acceptable $\Delta L_c/r$ of 6%. Then eqns (14), (10) and (25) give

$$\sigma_c^+/p = 6.35, \sigma_{cm}^+/p = 7.90, \tag{31}$$

for $\mu = 0.4$.

For the hoop stress σ_h, there are three contributions: nominal stresses from the force *F* of fig. 1, stresses produced by the contact stress σ_c, and stresses generated by the shear stress τ_c. We treat each of these in turn.

Balancing vertical forces for uniform normal stresses in rectangular and cylindrical polar coordinates, when the two coordinate systems share a common origin at the intersection of the projections of the contact flats in fig. 1, directly yields an estimate of the nominal hoop stress, σ_{hn}, at the edge of contact. Thus

$$\sigma_{hn} = F/w, \tag{32}$$

for $x = L_c/2$, where *w* is the width of the blade cross section at *C* (fig. 1). For locations immediately above the edge of contact, *w* in eqn (32) is reduced and the nominal hoop stress becomes

$$\sigma_{hn}^+ = \frac{F}{w + (L_c - 2x)\cos\alpha}, \tag{33}$$

wherein now the plus sign indicates *x* slightly in excess of $L_c/2$. Conversely, within the contact area, *w* is increased. In addition, *F* is reduced by virtue of being increasingly balanced by forces on the contact flats. Because these nominal stresses transpire to be an order of magnitude less than the complete hoop stress, we just model these reductions in *F* with a linear fit, and take

$$\sigma_{hn}^- = \frac{F(L_c + 2x)}{2L_c\left[w + (L_c - 2x)\cos\alpha\right]}, \tag{34}$$

for $|x| < L_c/2$, as the minus sign on σ_{hn} indicates.

Contact stresses simply produce exactly the same lateral surface stresses in 2D elasticity. This is a consequence of Michell's solution in [13] for the strip loading of an elastic half plane that has the same equality of normal stresses in

the surface. Hence, absent friction, the hoop stress acting in fig. 2 for the dovetail attachment of fig. 1 is given by

$$\sigma_h = \begin{cases} \sigma_{hn}^{+} & \text{for } x > L_c/2, \\ -\sigma_{cm} + \sigma_{hn}^{-} & \text{for } x < L_c/2, \end{cases} \tag{35}$$

and it is understood that x only slightly exceeds $L_c/2$ for the upper result.

When the shear stresses attending friction act in the positive sense shown in fig. 2, they generate tensile hoop stresses at C, compressive at C'. These stresses can be obtained by superimposing stresses from the Boussinesq horizontal line load on an elastic half plane. Thus from, for example, Johnson [4], p. 19, and eqn (30), the additional hoop stress, $\Delta\sigma_h$, generated by frictional shear stresses is given by

$$\Delta\sigma_h = \frac{2\mu}{\pi} \int_{-L_c/2}^{L_c/2} \frac{\sigma_{cm}(\xi)}{x - \xi} \mathrm{d}\xi, \tag{36}$$

where $\sigma_{cm}(\xi)$ is σ_{cm} of eqn (27) with ξ replacing x.

With a view to clarifying the key contribution stemming from the integral in eqn (36), we exchange σ_{cm} for $\sigma_{Hm} + \sigma_{cm} - \sigma_{Hm}$, where σ_{Hm} is σ_H of eqn (17) with σ_c^{+} replaced by σ_{cm}^{+}. Then the integral involving σ_{Hm} can be evaluated analytically: see Poritsky [14]. Denoting the hoop stress from this integral by $\sigma_{H\mu}$, we have

$$\sigma_{H\mu} = 2\mu\sigma_{cm}^{+} \begin{cases} \overline{x} - \sqrt{\left(\overline{x}^2 - 1\right)} & \text{for } \overline{x} > 1, \\ \overline{x} & \text{for } \overline{x} < 1, \end{cases} \tag{37}$$

where $\overline{x}$ remains as in eqn (17). Hence in conjunction with eqn (35) we have, for the edge-of-contact hoop stress distribution with friction present,

$$\sigma_h = \begin{cases} 2\mu\sigma_{cm}^{+}\left(\overline{x} - \sqrt{\left(\overline{x}^2 - 1\right)}\right) + \sigma_{h\mu} + \sigma_{hn}^{+} & \text{for } 1 \le \overline{x} \le 2, \\ 2\mu\sigma_{cm}^{+}\overline{x} + \sigma_{h\mu} - \sigma_{cm} + \sigma_{hn}^{-} & \text{for } |\overline{x}| \le 1, \end{cases} \tag{38}$$

where

$$\sigma_{h\mu} = \frac{2\mu}{\pi} \int_{-L_c/2}^{L_c/2} \left[\sigma_{cm}(\xi) - \sigma_{Hm}(\xi) H\left(\xi - x^{+} + \Delta x^{+}\right)\right] \frac{d\xi}{x - \xi}, \tag{39}$$

and H is the Heaviside unit step function. What eqn (38) then shows is that σ_h has an infinite positive gradient as $\overline{x} \to 1, \overline{x} > 1$, from the first term in the upper line, as well as an infinite negative gradient as $\overline{x} \to 1, \overline{x} < 1$ corresponding to

$x \to L_c/2, x < L_c/2$, from σ_{cm} of eqn (10) which contains $\sin\phi = \sqrt{\left(1-\left(2x/L_c\right)^2\right)}$. It follows that the maximum value of the hoop stress occurs right at the edge of contact and is given by

$$\sigma_h^+ = 2\mu\sigma_{cm}^+ + \sigma_{h\mu}\left(x = L_c/2\right) + \sigma_{hn}, \tag{40}$$

where σ_{hn} is as in eqn (32). For the friction case of eqn (4), we compute these various contributions to σ_h^+ (using a midordinate rule in conjunction with singularity programming to calculate the Cauchy principal value of the integral for σ_{hn} in eqn (39)). Normalized by *p*, the following results are given for the terms in eqn (40) in the order which they occur there:

$$\sigma_h^+/p = 6.32 + 1.36 + 0.82 = 8.50. \tag{41}$$

As expected from the nature of the expressions in eqn (38), the first term in eqn (41) is the major contributor to the peak hoop stress.

6 Validation of the analytical approach

The preceding analytical approach makes a number of simplifying assumptions. Accordingly we seek to evaluate the validity of this approach by comparing with an accurate finite element determination of corresponding stresses. To this end we choose the FEA of Sinclair *et al*. [1] because there, by refining meshes sufficiently, converged contact stresses for the dovetail attachment of fig. 1 are reported.

The FEA in [1] employs four-node quadrilateral elements in concert with point-to-surface contact elements (PLANE42 and CONTAC48, ANSYS [15]). For these elements, once contact extents have been determined, errors in stresses, e_σ, behave like

$$e_\sigma = O(h) \text{ as } h \to 0, \tag{42}$$

where *h* is the element size in the vicinity of where σ is being determined.

The initial mesh (*m* = 1) used in [1] features significant mesh gradation away from the contact region, but nearly constant element sizes within the vicinity of the contact region with *h* equaling about 16% of the edge radius *r*. This mesh is refined by halving element extents to produce two further meshes (*m* = 2, 3). Thereafter, to reduce computational effort, the submodelling technique of Cormier *et al*. [16] is employed in the neighborhood of *C* in fig. 1 wherein the maximum contact stresses occur. This results in three additional meshes (*m* = 4-6) with element sizes continuing to be halved.

For the first three meshes, contact extents vary, as do the locations of peak contact stresses. Consequently contact stresses are not expected to have

converged on this first sequence of meshes, and indeed, as is apparent in what follows, this proves to be the case. Nonetheless, the finest of these three meshes furnishes the best estimates available of the relative contributions of bending to peak contact stresses because such estimates are not available from the submodel meshes since they focus on the contact stress at C alone. For this mesh (m = 3) then, averaging peak contact stresses at C and C' and dividing into the peak at C by itself furnishes

$$\sigma_{cm}^{+}/\sigma_{c}^{+} = 1.2,1.3, \tag{43}$$

for μ = 0.0, 0.4, respectively. Despite underlying contact stresses for the ratios in eqn (43) not being converged, the ratios are quite comparable to their counterparts with the analytical approach in eqn (25) (within 5%).

On the three submodel meshes, contact extents in [1] are adjusted by successively smaller amounts with mesh refinement and appear to have converged with contact extensions being about 1% of the extent of the contact flat corresponding to λ = 0.98. This is also quite comparable to results for the analytical approach (e.g., eqn (13)). Further, the locations of the peak contact stresses remain fixed on all three submodel meshes and coincident with that for m = 3 (see figs 4(b) and 5(a), [1]). Hence on this entire sequence of four meshes a reasonable determination of the extent to which the FEA has converged is possible. Table 1, therefore, includes the peak contact stresses for m = 3-6 from [1] (specifically, from Table 2 thereof on renormalizing).

Table 1: Finite element results for edge-of-contact stresses.

Mesh, m	Mesh size, h/r	σ_{cm}^{+}/p μ = 0.0	σ_{cm}^{+}/p μ = 0.4	σ_{h}^{+}/p μ = 0.4
3	1/25	5.53	6.26	3.99
4	1/50	5.95	6.96	4.95
5	1/100	6.16	7.23	5.83
6	1/200	6.26	7.36	6.50
“∞”	“0”	6.36	7.49	(8.64)
Corresponding analytical value:		6.30	7.90	8.50

For the peak contact stresses in Table 1 for $\mu = 0.0$, stress increments successively halve with mesh refinement, or nearly so. Such numerical results are consistent with a linearly converging analysis. Thus Richardson extrapolation [17] for linear convergence can be applied and merely adds the last stress increment to the last stress (m = 6) to get an extrapolated value. These values loosely correspond to $m \to \infty$ or $h \to 0$, and are included in Table 1. The same situation obtains for meshes m = 4, 5, 6 for $\mu = 0.4$, and extrapolated values are likewise included.

With linear convergence, discretization errors in stresses do behave as in eqn (42). Hence percentage errors for mesh m results, $\in_m$, can be estimated by

$$\in_m = \frac{\Delta\sigma_m}{\sigma_m} \text{x}\, 100(\%), \tag{44}$$

where $\Delta\sigma_m = \sigma_m - \sigma_{m-1}$, σ_m being the FEA determination of the stress of concern on mesh m. Applying eqn (44) to the results in Table 1 for σ^+_{cm} gives $\in_6 = 1.6\%, 1.8\%,$ for $\mu = 0.0,\ 0.4,$ respectively. All told, therefore, it would seem reasonable to regard the FEA results of [1] for σ^+_{cm} as being of good accuracy.

For comparison, corresponding analytical results for σ^+_{cm} from eqns (16) and (31) are also included in Table 1. The analytical result for σ^+_{cm} for $\mu = 0.0$ agrees well with the extrapolated FEA result (within 1%). The analytical result for $\mu = 0.4$ agrees satisfactorily with the extrapolated FEA result (within 6%). The greater disagreement for the latter case is perhaps to be expected because the presence of friction increases the complexity of the contact configuration and consequently results in additional simplifications in the analytical approach (see Section 5). It also challenges the FEA more: despite the FEA indicating that slip occurs throughout the contact region, peak shear contact stresses diverge from satisfying Amonton's law by 3.3% in [1], so that perhaps errors in σ^+_{cm} for $\mu = 0.4$ are somewhat larger than the 1.8% estimate made using eqn (44). In all, therefore, at least a satisfactory validation of the analytical approach.

While not part of the validation of the analytical approach, FEA hoop stresses are in addition included in Table 1 to illustrate the challenges of determining this stress right at the edge of contact with finite elements. In contrast to contact stresses, peak hoop stress locations are a never coincident throughout the mesh sequence (see fig. 5(b), [1]), and only for m = 6 occur at the correct location ($x = L_c$). Consequently stress increments vary erratically rather than systematically and are not in agreement with increments for linear convergence. Because these increments are decreasing in magnitude, it is possible to apply generalized Richardson extrapolation as in Roache [18], on p. 111. This leads to the value included in parentheses in Table 1: parentheses are used because experience has shown that such large changes with extrapolation can be unreliable. Rather, instead, we use the increments to estimate the error with a procedure that

recognizes erratic convergence. In accord with Roache [18], p. 155, this procedure has, for mesh refinement halving element extents,

$$\in_m = \frac{\Delta\sigma_m}{\sigma_m\left(2^{c_m}-1\right)} \text{x}\, 100(\%), \tag{45}$$

where $c_m = \ln\left(\Delta\sigma_{m-1}/\Delta\sigma_m\right)/\ln 2$ is an estimate of the effective convergence rate. Applying eqn (45) to the results in Table 1 for σ_h^+ gives $\in_6 = 33\%$. Alternatively, if one were to take the analytical value from eqn (41) given in Table 1 as being accurate, $\in_6 = 24\%$. Either way, the error level in σ_h^+ is not satisfactory.

There are reasons why the FEA determination of σ_{cm}^+ can be accurate but that for σ_h^+ not be. For σ_{cm}^+, while it is near an infinite stress gradient at $x = L_c$, at $x = x^+$ the actual stress gradient in σ_{cm} is zero. In contrast, the stress gradients for σ_h at its peak location, $x = L_c$, are infinitely positive then infinitely negative as L_c is approached from above and below (see Section 5). These severe gradients seriously impair the determination of σ_h^+ with finite elements. For peak hoop stresses, therefore, the analytical approach may offer a significantly more effective means of determining such stresses than FEA.

7 Concluding remarks

Drawing on the contact stress solution in Shtaerman [2], an analytical approach is developed for blade attachments in gas turbines. The approach enables the FEA of such attachments to determine just stress resultants, quantities that converge more rapidly than stresses themselves. Given the appropriate resultants, the approach then furnishes key edge-of-contact stresses.

The analytical approach employs a number of simplifying assumptions. To check the validity of these assumptions, peak contact stresses are compared with an FEA that has converged corresponding stresses. Agreement between the two is quite satisfactory (differences < 6%).

Results for the edge-of-contact stresses show that significant stress concentrations occur near the edge of contact. The most potentially damaging of these stress raisers is a tensile hoop stress that occurs right at the edge of contact. This stress is likely to be the most damaging because, as the analytical approach explicitly shows, it has severe stress gradients when approached from either inside or outside of contact. As a result, small changes in operating rpm and nominal stresses produce relatively large changes in this hoop stress as the contact region shifts.

Focusing, therefore, on this key hoop stress at the edge of contact, there are several options for reducing its severity. Shot peening can be used to reduce its magnitude by adding a compressive contribution. Choosing materials that are

otherwise equivalent in terms of strengths in the turbine environment but have a lower coefficient of friction lower this stress largely proportionally. And precision crowning as in Sinclair and Cormier [19] offers a potential means of completely removing peak hoop stresses at the edge of contact.

Acknowledgement

The benefit of technical discussions with Dr J. H. Griffin of Blade Diagnostics Corporation during the course of preparing this study is gratefully acknowledged.

References

[1] Sinclair, G.B., Cormier, N.G., Griffin, J.H. and Meda, G., Contact stresses in dovetail attachments: finite element modeling. *Journal of Engineering for Gas Turbines and Power*, **124**, pp. 182-189, 2002.
[2] Shtaerman, I.Y., *Contact Problems of the Theory of Elasticity*, Gostekhizdat Publishing: Moscow, 1949 (in Russian: an English translation is available from the Foreign Technology Division of the British Library, FTD-MT-24-61-70, 1970).
[3] Hamdy, M.M. and Waterhouse, R.B., The fretting wear of Ti-6Al-4V and aged Inconel 718 at elevated temperatures. *Wear*, **71**, pp. 237-248, 1981.
[4] Johnson, K.L., *Contact Mechanics*, Cambridge University Press: Cambridge, U.K., 1985.
[5] Hertz, H., On the contact of elastic solids. *Journal für die Reine und Angewandlte Mathematik*, **92**, pp. 156-171, 1882 (in German: for an account in English, see [4], Ch. 4).
[6] Steuermann, E., To Hertz's theory of local deformation in compressed elastic bodies. *Comptes Rendus (Doklady) de l'Académie des Sciences de l'URSS*, **25**, pp. 359-361, 1939.
[7] Persson, A., On the stress distribution of cylindrical elastic bodies in contact. Doctoral dissertation, Chalmers Tekniska Hogskola, Göteborg, Sweden, 1964.
[8] Gladwell, G.M.L., *Contact Problems in the Classical Theory of Elasticity*, Sijthoff and Noordhoff: Alphen aan den Rijn, The Netherlands, 1980.
[9] Sinclair, G.B. and Cormier, N.G., Contact stresses in dovetail attachments: physical modeling. *Journal of Engineering for Gas Turbines and Power*, **124**, pp. 325-331, 2002.
[10] Sadowsky, M.A., Two-dimensional problems of elasticity theory. *Zeitschrift für Angewandte Mathematik und Mechanik*, **8**, pp. 107-121, 1928 (in German: for an account in English, see [4], Ch. 2).
[11] Griffin, J.H. and Cushman, M., Private communication, 2012.
[12] Muskhelishvili, N.I., *Some Basic Problems of the Mathematical Theory of Elasticity*, P. Noordhoff Ltd.: Groningen, The Netherlands, 1963.
[13] Michell, J.H., The inversion of plane stress. *Proceedings of the London Mathematical Society*, **34**, pp. 134-142, 1902.

[14] Poritsky, H., Stresses and deflections of cylindrical bodies in contact. *Journal of Applied Mechanics*, **17**, pp. 191-201, 1950.
[15] ANSYS personnel, *ANSYS User's Manual*, Revision 5.2, ANSYS Incorporated: Canonsburg, Pennsylvania, 1995.
[16] Cormier, N.G., Smallwood, B.S., Sinclair, G.B. and Meda, G., Aggressive submodelling of stress concentrations. *International Journal for Numerical Methods in Engineering*, **46**, pp. 889-909, 1998.
[17] Richardson, L.F., The approximate arithmetical solution by finite differences of physical problems involving differential equations, with an application to the stresses in a masonry dam. *Philosophical Transactions of the Royal Society*, **A210**, pp. 307-357, 1910.
[18] Roache, P.J., *Fundamentals of Verification and Validation*, Hermosa Publishers: Socorro, New Mexico, 2009.
[19] Sinclair, G.B. and Cormier, N.G., Contact stresses in dovetail attachments: alleviation via precision crowning. *Journal of Engineering for Gas Turbines and Power*, **125**, pp. 1033-1041, 2003.